INTERNATIONAL JOURNAL OF HYDROGEN ENERGY 47 (2022) 29184–29194

Available online at www.sciencedirect.com

ScienceDirect

journal homepage: www.elsevier.com/locate/he

The evolution and structure of ignited high-pressure cryogenic hydrogen jets

Zhaoxin Ren [a,b], *Stella Giannissi* [c], *A.G. Venetsanos* [c], *A. Friedrich* [d], *Mike Kuznetsov* [e], *T. Jordan* [e], *Jennifer X. Wen* [a,*]

[a] *Warwick FIRE, School of Engineering, University of Warwick, Coventry, CV4 7AL, UK*
[b] *Zienkiewicz Centre for Computational Engineering, Faculty of Science and Engineering, Swansea University, Swansea, SA1 8EN, UK*
[c] *Environmental Research Laboratory, National Centre for Scientific Research Demokritos, Aghia Paraskevi, Athens, 15341, Greece*
[d] *Pro-Science GmbH, Parkstrasse 9, Ettlingen, 76275, Germany*
[e] *Karlsruhe Institute of Technology, 44, Eggenstein-Leopold, 76344, Germany*

HIGHLIGHTS

- Numerical predictions reveal insight of the transient ignition, flame structures and dynamics.
- The near-field ignition led to a side diffusion flame and mostly unignited inner cold core.
- The far-field ignition resulted in a diffusion flame at outer edge and a premixed flame inside the jet.
- Localized spontaneous ignition and transient flame extinguishment were predicted during the evolution.
- The predictions also captured the experimentally observed deflagration waves in the far-field ignited jets.

ARTICLE INFO

Article history:
Received 22 April 2022
Received in revised form
16 June 2022
Accepted 24 June 2022
Available online 12 August 2022

Keywords:
High-pressure cryogenic hydrogen
Large eddy simulation
Ignited hydrogen jet
Flame evolution and structure

ABSTRACT

The anticipated upscaling of hydrogen energy applications will involve the storage and transport of hydrogen at cryogenic conditions. Understanding the potential hazard arising from leaks in high-pressure cryogenic storage is needed to improve hydrogen safety. The manuscript reports a series of numerical simulations with detailed chemistry for the transient evolution of ignited high-pressure cryogenic hydrogen jets. The study aims to gain insight of the ignition processes, flame structures and dynamics associated with the transient flame evolution. Numerical simulations were firstly conducted for an unignited jet released under the same cryogenic temperature of 80 K and pressure of 200 bar as the considered ignited jets. The predicted hydrogen concentrations were found to be in good agreement with the experimental measurements. The results informed the subsequent simulations of the ignited jets involving four different ignition locations. The predicted time series snapshots of temperature, hydrogen mass fraction and the flame index are analyzed to study the transient evolution and structure of the flame. The results show that a diffusion combustion layer is developed along the outer boundary of the jet and a side diffusion flame is formed for the near-field ignition. For the far-field ignition, an envelope flame is observed. The flame structure contains a diffusion flame on the outer edge and a premixed flame inside the jet. Due to the complex interactions between turbulence, fuel-air mixing at cryogenic temperature and chemical reactions, localized spontaneous

* *Corresponding author.*
E-mail address: jennifer.wen@warwick.ac.uk (J.X. Wen).
https://doi.org/10.1016/j.ijhydene.2022.06.230

ignition and transient flame extinguishment are observed. The predictions also captured the experimentally observed deflagration waves in the far-field ignited jets.

Introduction

Hydrogen is an essential element in the global energy transition towards zero-emission. Although hydrogen has the highest energy per mass of any fuel, its volumetric energy density is low. The upscaling of hydrogen energy applications requires the storage of relatively large quantities of hydrogen, which can be achieved through either high-pressure or low-temperature systems. In this regard, cryo-compression is a competitive technique [1]. Hydrogen can be stored in a vessel at cryogenic temperatures as low as 20 K and high pressures up to 35 MPa. High-pressure cryogenic hydrogen generally refers to compressed hydrogen gas below 120 K. Their accidental leak will lead to the formation of under-expanded jets and jet flames if ignited. Delayed ignition can also lead to hydrogen explosion. Understanding potential accidental scenarios associated with high-pressure cryogenic hydrogen is important to help ensure its safe handling.

Few experiments have been performed to study ignited cryogenic hydrogen jets. Veser et al. [4] studied hydrogen jet flames from pressurized release at cryogenic temperatures between 35 and 80 K, and considered the effects of release pressure, nozzle diameter, and ignition position. Friedrich et al. [5] experimentally investigated ignited cryogenic hydrogen jets from 7 to 35 bar releases in the temperature range of 34–65 K. They analyzed the flame stability, combustion regimes, and thermal radiation. Panda and Hecht [6] investigated the ignition characteristics of round hydrogen jets from 2 to 6 bar releases at 37–295 K. Comparing with releases at ambient temperature, both the maximum ignition distance from the nozzle and the flame length of the high-pressure cryogenic hydrogen jets were found to increase, implying that accidently released high-pressure cryogenic hydrogen is prone to ignition further away from the release source in comparison with ambient temperature. Hecht and Chowdhury [7,8] studied the effects of aspect ratio for the rectangular nozzle and found that it had no obvious effect on the distribution of hydrogen concentration and flame size.

Numerical simulations of cryogenic jets have been conducted in several recent studies [2,9–12]. Limited studies have addressed the ignited releases, which can lead to either jet fires or deflagration in some situations. Cirrone et al. [1] numerically studied cryogenic hydrogen jet flame using Reynolds Averaged Navier Stokes (RANS) approach for the experimental conditions of Panda and Hecht [6]. The predictions captured the changing trend of flame length and radiant heat flux. Cirrone et al. [13] recently considered cryo-compressed ignited hydrogen horizontal releases and numerically predicted the thermal radiation hazards.

More recently, a series of large-scale experiments were conducted for ignited jets released at a cryogenic temperature of 80 K and pressure from 5 to 200 bar in the Pre-normative REsearch for Safe Use of Liquid HYdrogen (PRESLHY) project, funded by the Fuel Cell and Hydrogen Joint Undertaking of the European Commission [14]. Different ignition locations from 0.4 to 2.0 m from the nozzle were considered. The ignition delay time ranged from 80 to 160 ms. Depending on the ignition delay time and location, the flame was found to either burn back to the nozzle and sustained after the ignition source was turned off, or it only propagated upwards and quenched once the ignition source was turned off. A strong explosion with the formation of a spherical shock wave occurred just after ignition in some tests.

The present study aims to numerically characterize ignited cryogenic hydrogen jets, focusing on the transient flame dynamics and flame structures using large eddy simulation techniques (LES). The numerical simulations were set up using the experimental configuration in PRESLHY [14] but before the detailed test conditions and results become available. Some comparisons with the experimental observations/measurements will be presented. The predictions have captured fine details of the ignition and flame evolution processes which are difficult to quantify in large-scale experiments.

Numerical model

The numerical simulations are conducted with rhoReactingFOAM [15], which is a compressible reacting flow solver within the frame of open-source computational fluid dynamics (CFD) code OpenFOAM. Detailed description of the methodology can be found in [15]. Briefly, all variables are decomposed into resolved and unresolved subgrid scale (SGS) components by spatially filtering the reactive Navier-Stokes equations. The Favre-filtered governing equations are solved for mass, momentum, and total enthalpy and chemical species. Turbulent viscosity is calculated using the one eddy equation model of Yoshizawa [16]. The adopted LES approach is well suited to consider the transient ignition and fire features as demonstrated in the authors' previous studies [26]. Comparing with the RANS approach previous used to simulate cryogenic hydrogen jet fires [1], the LES approach can better capture the transient evolution of the flame kernel. The modified eddy dissipation concept (EDC) of Parente et al. [17] is used for combustion along with a detailed kinetic scheme involving 9 species and 19 steps [18].

The use of the finite-rate chemistry facilitates the consideration of non-unity Lewis number, local extinction and

reignition as well as different modes of combustion. The semi-implicit Bulirsh-Stoer (SIBS) method is used for the ordinary differential equation (ODE) in chemistry. Thermodynamic properties are calculated using the NIST equation of state based on explicit modeling of the Helmholtz free energy and considered as the current standard for cryogenic hydrogen [9]. The molecular transport model of Burali N et al. [25] is used. It considers non-unity Lewis number effect by calculating mass diffusivity based on species Lewis number and thermal diffusivity. The model for thermal and transport properties is expected to influence the dispersion and spatial distribution of hydrogen.

The radiative heat transfer equation is solved by the finite volume discrete ordinates method with the weighted sum of grey gases model for the radiative properties of the gases [19].

Fig. 1 shows the three-dimensional (3D) cylindrical computational domain, which is of 2 m in diameter and 3 m high. The set up was based on pre-calculations of an unignited high-pressure cryogenic jet and further checked with preliminary simulations to confirm no significant velocities at the boundaries. The side, top, and bottom boundaries of the domain are set as open with no influence on the flow across the domain. The circular hydrogen inlet is at the center of the bottom plane (x-y plane, $z = 0$). The simulations were set up with the same initial pressure of 200 bar and cryogenic temperature of 80 K as in PRESLHY experiments [14] for a nozzle diameter of 4 mm. Due to the high release pressure, the ejected hydrogen forms an under-expanded jet. Pre-calculations were conducted using a notional nozzle model previously validated for similar high-pressure cryogenic hydrogen releases [9] to estimate the flow conditions when the jet expanded to the ambient pressure. The cryogenic notional nozzle approach is used to bypass the shock-laden under-expanded region. Simulation starts from a pseudo position where the jet has expanded to ambient pressure for computational efficiency. As the length of the under-expanded region is shorter than the closest ignition position of 0.5 m, this simplification has relatively little effect on the flame simulation and often used in simulating large-scale jet fires. High-pressure cryogenic hydrogen is injected from the center of the bottom along the z-direction with the velocity and temperature calculated by the notional nozzle model. The domain is initially filled with stagnant air at 300 K and ambient pressure.

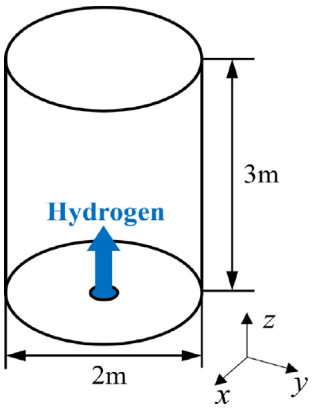

Fig. 1 – Schematic diagram of the computational domain.

A structured grid with 40 million cells is used with the smallest filter width of $\Delta = 1$ mm located in the near-field region. This means that the eddy with the size above 1 mm is resolved and SGS turbulence is assumed to be isotropic and homogeneous. Local mesh refinement is applied in the shear layer between the jet and ambient air to resolve most of the turbulent kinetic energy. In particular, the characteristic fire diameter, D^*, is calculated to guide the grid resolution Δ. $D^*/\Delta > 15$ in the present study is found adequate for a wide range of simulations in Ref. [22]. The chosen grid spacing of 1 mm gives $D^*/\Delta = 200$, which is much finer to mimic the jet flow. The Courant–Friedrichs–Lewy (CFL) numbers are kept to be less than 0.5 in the entire computational domain, corresponding to a physical time step in the order of 0.1 μs. The computation is performed using 1000 cores on the UK Engineering and Physical Science Research Council's ARCHER2 Supercomputer. Table 1 lists the 4 ignition locations considered. This mimics the experimental arrangements [14], in which the ignition location, z_{ig}, was set on different streamwise positions along the centerline to investigate its influence on the transient flame propagation. Hereafter, Cases F05 and F10 will be referred to as near-field ignition while Cases F15 and F20 as far-field ignition, in which the jets have evolved further at the time of ignition. The ignition source is set as a cube with a side length of 2 cm. Its temperature T_{ig} is set to 2000 K, which is close to the adiabatic flame temperature of stoichiometric hydrogen-air mixture. The ignition source contains hot air throughout the simulation. This was set from the beginning and hence ignition delay is not considered. The ignition time followed that in the experiments, which tried a variety of ignition delay time ranging from 80 ms to 160 ms, before choosing 120 ms for most of the tests including the ones considered in the present study [20]. An unignited cryogenic hydrogen jet, named UF, is also simulated for some validation.

Results and discussion

Cold flow

For the cold flow without ignition (Case UF), the evolution of the cryogenic hydrogen jet is simulated. The snapshots of the spatial distributions of hydrogen mole fraction are provided in Fig. 2. At time $t = 1$ ms, the hydrogen jet penetrates the ambient still air and the jet tip has a regular round shape, as shown in Fig. 2(a). With further evolution of the flow, the jet tip becomes corrugated. Some vortices are formed around the jet due to the shear between the high-speed jet and ambient air with zero velocity. In Fig. 2(b), with hydrogen at the corrugated edge of the jet starting to mix with the surrounding air, its concentration decreases. At $t = 20$ ms in Fig. 2(c), the

Table 1 – Summary of the ignition locations considered.

Case #	UF	F05	F10	F15	F20
Ignition location, z_{ig} (m)	/	0.5	1.0	1.5	2.0

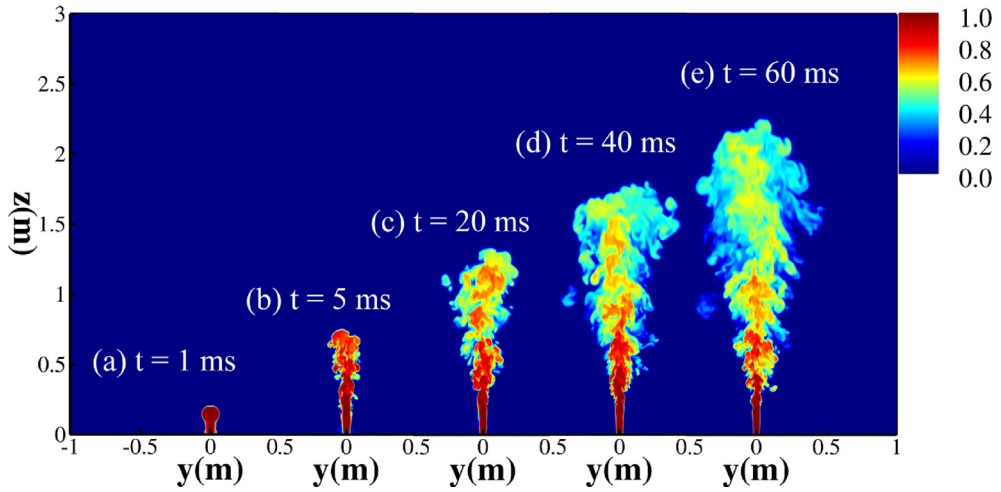

Fig. 2 – Instantaneous distributions of hydrogen mole fraction at y-z middle-plane for Case UF with different times.

mixing between hydrogen and surrounding air leads to further dilution. Due to momentum transfer from hydrogen to ambient air, the penetration speed of the jet decreases continuously. The formed large-scale vortices entrain ambient air into the expanding jets to accelerate the mixing process, as depicted in Fig. 2(d) and (e). Flammable mixture is formed at some distance from the nozzle and the extent of the flammable region increases rapidly with time.

The predicted axial hydrogen concentration statistics of the unignited jet (Case UF) are compared with the measurements of Friedrich et al. [21] in Fig. 3, in which X_{H2} is the axial centerline hydrogen mole fraction and z (m) represents the streamwise positions. The experiments measured hydrogen mole fractions at 0.5, 1.0 and 1.5 m along the centerline. Some small discrepancies exist between the predicted and measured concentrations. This is likely due to the small difference in the turbulence level at the inlet boundaries. In the numerical simulation, it was specified as 5% while the level of turbulence at nozzle exit in the experiment was not characterized. Nevertheless, the differences are very small and the present solver is validated to simulate the hydrogen dispersion. The predictions serve to inform the setup of the subsequent numerical simulations of the ignited jets.

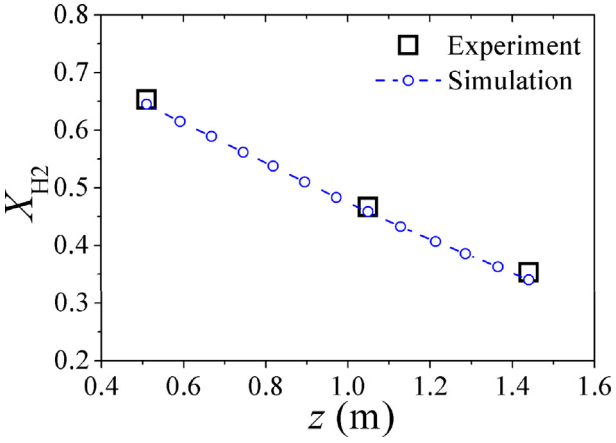

Fig. 3 – Comparisons of predicted and measured axial hydrogen concentration [21].

Transient flame evolution

Following successful ignition, the typical development of an ignited flame experiences several stages including flame kernel growth, radial expansion, and flame propagation [23]. The present study is focused on the transient flame evolution in the ignited cryogenic hydrogen jets. As shown in Table 1, four ignition positions are considered. As the cryogenic hydrogen jet disperses downstream, the hydrogen concentration decreases due to air entrainment and mixing of fuel and air, which leads to the formation of flammable mixture. The different ignition locations lead to variations in the flame characteristics. The predictions for the near-field ignition (z_{ig} = 0.5 m) are shown in Fig. 4. The near-field ignition encounters a relatively cold mixture with relatively high hydrogen concentration.

Earlier experimental studies of Wierzba and Ale [27] indicated that an initial temperature increase from 273 K to about 620 K has a slight influence on the hydrogen flammability. However, the recent experimental investigations of Proust and Jamois [28] revealed that the flammability range decreases when the temperature drops, especially the upper flammability limit (UPL) reduced to 60 and 66% vol. and lower limit of hydrogen flammability (LFL) increased to 5.6 and 6, respectively when the hydrogen gas temperature dropped to 213 K and 153 K, respectively. No measurements are available for the considered cryogenic release temperature of 80 K considered in the present study. However, as the actual temperature of the jet increase due to heat exchange with the surrounding air following release, Fig. 4 plots the iso-surface of hydrogen mole fraction of X_{H2} = 0.04 as a broad indication of the flammable region and jet structure. After the cold hydrogen jet interacts with the ignition source, a flame kernel forms at the jet tip. The edge flame grows during radial expansion around the jet tip, as shown in Fig. 4(a). Subsequently, the flame propagates upstream to envelop the jet. Due to the low temperature of the jet, there are still some

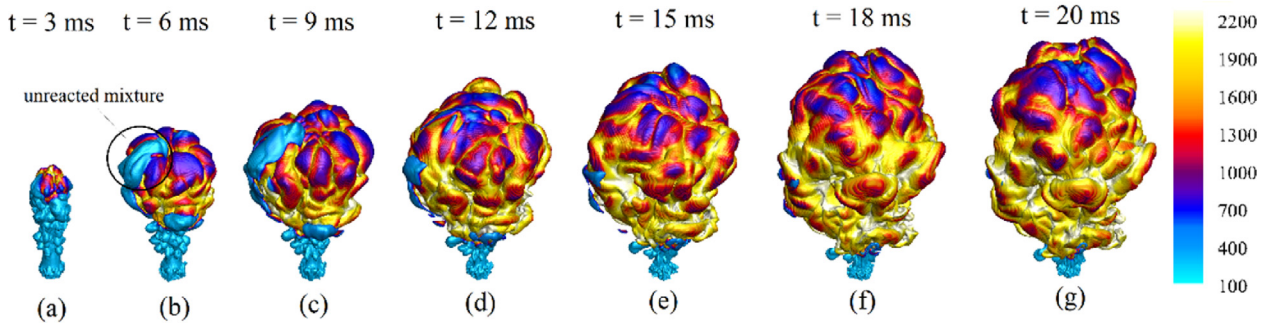

Fig. 4 – Transient evolution of ignited jet flame for Case F05 marked using $X_{H2} = 0.04$ iso-surface colored by temperature (K).

unreacted mixtures distributed on the top of the jet, as depicted by the temperature distributions on the hydrogen concentration iso-surface in Fig. 4(b). The flame temperature exhibits nonuniform spatial distribution. In particular, the flame distributed on the sides of the jet has a much higher temperature than the flame around the jet head. This is mainly because the shear on the sides of the jet contributes to heat transfer and species mixing of cold jet and warm surrounding air, providing a more favorable condition for chemical reaction. As the jet penetrates downstream, the unreacted area reduces and disappear at time $t = 18$ ms. Subsequently, the flame propagates upstream continuously and interacts with the oncoming air, resulting in wrinkled flame structure. Finally, the flame also propagates downwards towards the nozzle and almost wraps the whole jet.

Before analyzing the flame evolution in detail, the radial distributions of the temperature and mass fractions of hydrogen and oxygen are plotted in Fig. 5 along $z = 0.4$ m at $t = 3$ ms for Case F05 before ignition. The temperature distribution indicates that there is a very cold core in the jet center. From the jet center to the edge, the hydrogen concentration firstly increases briefly and then decreases rapidly while the temperature increases sharply towards the environment temperature. The mixing of the cold hydrogen and co-flow of entrained air is accompanied by intense heat transfer which increases the temperature of the reactive mixture at the jet edge. Due to the very low temperature in the jet center, ignition is expected to occur at the jet edge where temperature is relatively higher.

The global structure of the cryogenic jet flame is further illustrated by using the flame index, $FI = \nabla Y_{H2} \cdot \nabla Y_{O2}$ in Fig. 6 following the approach of Mizobuchi et al. [24]. The flame is premixed when FI is positive and diffusion when FI is negative. Fig. 6 presents the instantaneous flame structure obtained by the numerical simulation at the y-z middle-plane. The black isolines indicate the OH mass fraction $Y_{OH} = 0.001$. The OH radical distribution can characterize the spatial distribution of the flame front. In addition, the temperature distribution, associated with the OH radical, is shown in Fig. 7. A flame kernel (indicated as FK) is formed as the hydrogen jet tip interacts with the ignition source, as shown in Fig. 6(a) and Fig. 7(a). Then the edge flame propagates to warp the jet. These predictions indicate that a diffusion flame is formed for the near-field ignition as represented by the cyan region in Fig. 6. Fig. 7(c) indicates that a large amount of hydrogen inside the jet cannot be ignited due to the cryogenic temperature suppressing the chemical reaction. The flame front becomes corrugated from the vortex entrainment during the shear

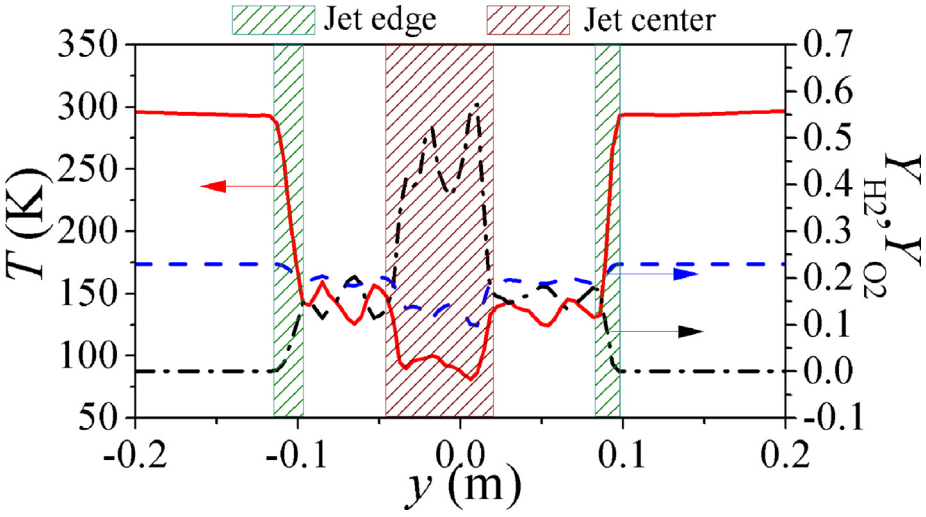

Fig. 5 – Radial profiles of temperature (red solid), H_2 (black dotdash) and O_2 (blue dashed) mass fraction at $t = 3$ ms for Case F05. (For interpretation of the references to colour in this figure legend, the reader is referred to the Web version of this article.)

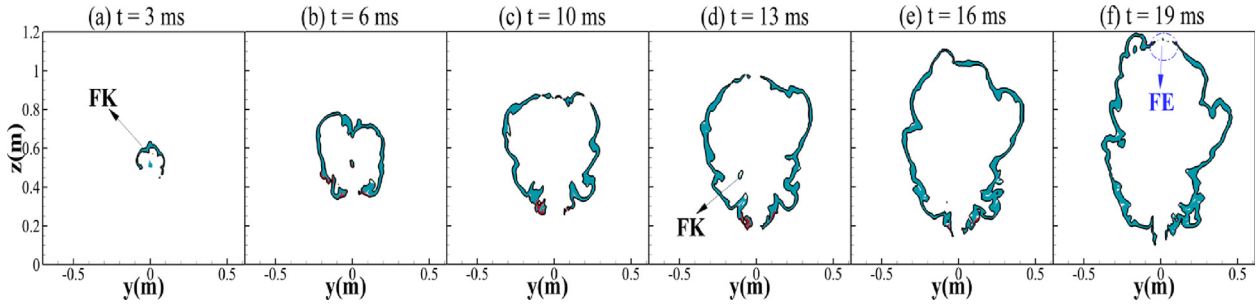

Fig. 6 – Evolution of flame structure at the y-z middle-plane for Case F05. Here, color shows the combustion mode, red: premixed, cyan: diffusion. The black isolines refer to OH mass fraction $Y_{OH} = 0.001$. DF, PF, FE, and FK are the abbreviations for diffusion flame, premixed flame, flame extinguishment, and flame kernel, respectively. (For interpretation of the references to colour in this figure legend, the reader is referred to the Web version of this article.)

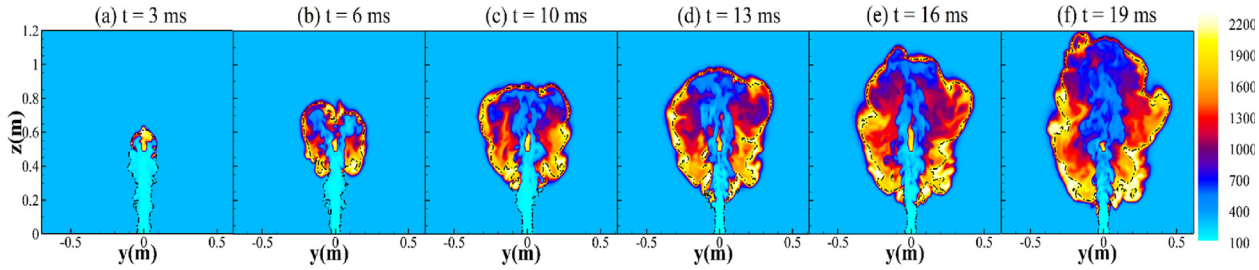

Fig. 7 – Evolution of combustion field at the y-z middle-plane for Case F05. Here, the contours are temperature (K), and the black dashed isolines refer to hydrogen mass fraction $Y_{H2} = 0.02$.

process along the sides of the jet. Another flame kernel is generated from the ignition source, as shown in Fig. 6(d), but subsequently it disappears. The details will be discussed later. Only a diffusion edge flame is formed. For the cryogenic hydrogen jet ignited closer to the nozzle, the flame front preferentially propagates outside the jet surface. This is because the turbulent shear flow generates fuel pockets with higher temperatures far from the jet center and these ignited pockets propagate faster than the main flame as the local velocity is relatively small. It is also found that a local flame extinguishment occurs at the top of the flame, as marked out in Fig. 6(f). This is mainly due to the influence from the cold jet dispersing upstream.

Fig. 8 illustrates the evolution of the flame kernel developed at the jet edge as shown in Fig, 6(d). The white rectangle indicates the regime where the flame kennel locates. As shown from the distributions of temperature, Y_{H2}, and Y_{O2}, at time $t = 12$ ms, the reactive mixture of hydrogen and oxygen with a high temperature provides a suitable condition for the formation of the flame kernel. At time $t = 13$ ms the kernel is already formed. Subsequently, the reactive mixture is consumed, and the kernel disappears, although the local temperature is high.

Fig. 9 shows the quenching process via the distribution of the OH mass fraction at 5 different instantaneous moments by different line types for Case F05. For all the instantaneous moments considered, OH radicals are only produced over a short section over the entire regions as differentiated by the height. At time $t = 6$ ms, the jet flame starts to form, and the flame kernel propagates downstream associated with the penetration of the jet flow. The chemical reaction is intense as reflected by the relatively high concentration of OH radicals at the jet tip. The peak values of the OH mass fraction dropped significantly at $t = 10$ and 13 ms; and then increased at $t = 16$ ms to about half of the initial peak values. The unsteady flow at the jet tip corrugates the flame surface, as shown in Fig. 6(e), resulting in an unstable jet flame. At $t = 19$ ms, quenching occurs at the jet tip. As shown by the profiles of the mass fractions of hydrogen and oxygen in Fig. 10. The flame is predominantly non-premixed as judged by the rapidly decrease of Y_{H2} and increase of Y_{O2} near the jet tip.

As the ignition location moves further away from the nozzle, ignition is easier as the mixture is less rich (see Fig. 2) and at higher temperature due to heat exchange with the environment. Fig. 10(a) shows the flame structure of Case F10 for ignition at $z_{ig} = 1.0$ m. After the kernel has fully grown from the ignition source, a flame front forms during the radial expansion and propagates upstream. Comparing with Case F05, the lift-off distance is longer for Case F10. The flame temperature also exhibits nonuniform distribution, in which the flame located on the sides of the jet has a higher temperature. However, the degree of nonuniformity is smaller than that in Case F05 due to the increasing exothermic reaction rates due to enhanced reactivity of the mixture at higher temperature.

Fig. 11 and Fig. 12 show the transient flame evolution of Case F10. The flame kernel forms at the jet tip and propagates outwards. But soon local extinction (marked as FE in Fig. 11(b)) occurs during the propagation of this diffusion flame front toward the negative y direction, as highlighted by the blue circle in Fig. 11(b). The disappearance of the flame front locates at the periphery of the vortex with an anticlockwise

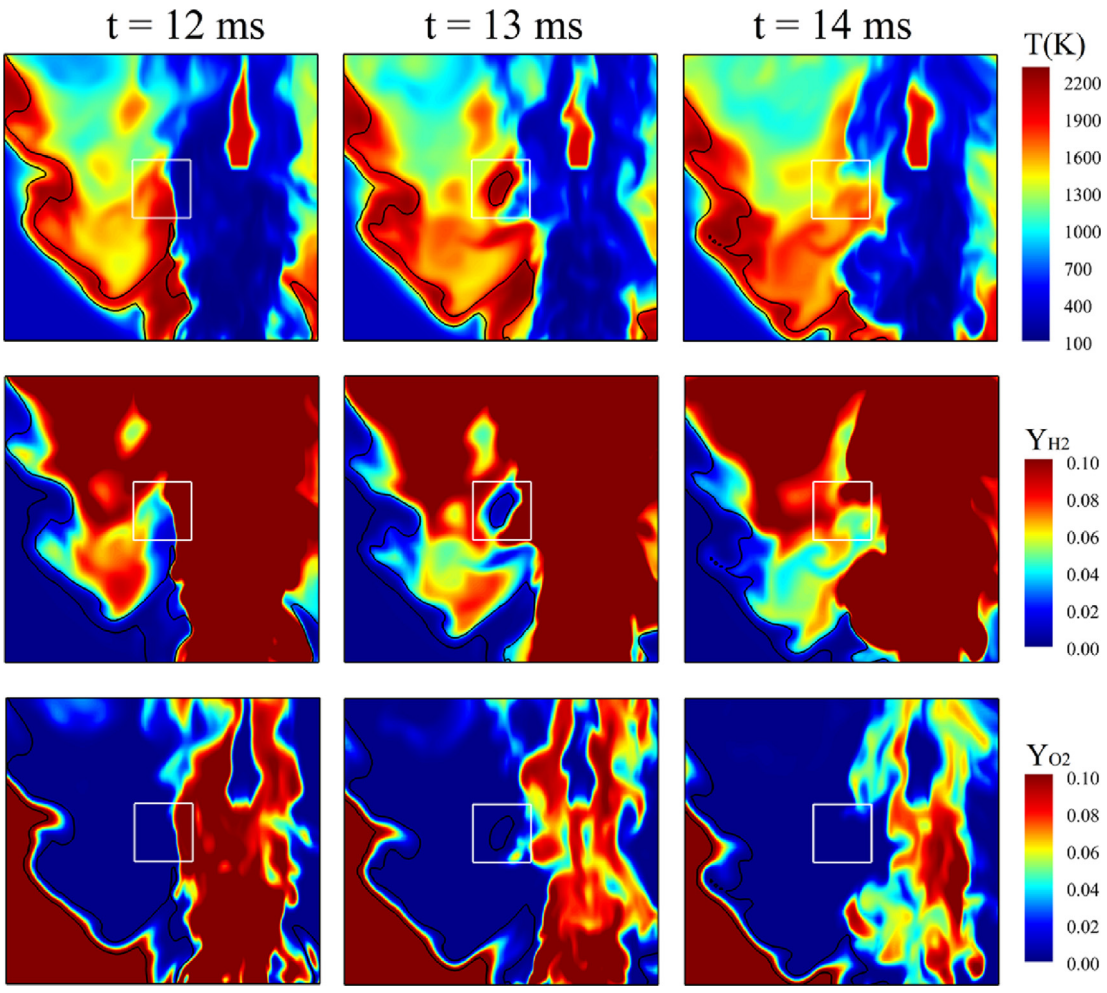

Fig. 8 – Formation and quenching of the flame kernel formed at the jet edge (Fig. 6(d)) for Case F05. The upper row shows temperature (T), the middle row shows hydrogen mass fraction (Y_{H2}), and the lower row shows the oxygen mass fraction (Y_{O2}). The black isolines refer to OH mass fraction $Y_{OH} = 0.001$. The white rectangle shows the regime where the kernel is formed.

rotation, as depicted by the local enlargement of the vorticity field. The local high dissipation rate due to the relatively high strain contributes to the quenching. The flame propagates along the jet sides and the high-temperature region expands toward the jet center and heats the local cold hydrogen, as shown in Fig. 12(c). Accordingly, some distributed flame kernels (FK), displaying a premixed mode, are formed in the core region spontaneously as depicted in Fig. 11(c) and (d). These scattered FKs cannot sustain the radial expansion and therefore a nonuniform temperature distribution appears in the core region, where cold unburnt mixture accumulates as shown in Fig. 12(f). For Case F10, although some premixed flame kernels are formed in the main jet, the global flame displays a diffusion structure. The flame front tends to propagate around the outer region of the jet. This is because that the shear on the sides of the jet promotes the mixing between hydrogen and air and increases the temperature of the local hydrogen-air mixture from the heat transfer. The flame evolution characteristics for cases F05 and F10 indicate that for the near-field ignition, the shear on the sides of the jet has important influences in the mixing and the transient flame evolution, which is controlled by turbulence from the shear layer.

For Case F15, the cold hydrogen jet is ignited further downstream ($z_{ig} = 1.5$ m). Fig. 10(b) shows that the temperature of the flame front is more uniform, and the lift-off distance increases further comparing with Case F10. As the jet interacts with the ignition source, a flame kernel is generated. The difference of the flame expansion from the near-field ignition is that the flame front can also propagates toward the inner core of the jet with a premixed combustion mode at an early stage, as shown in Fig. 13(a). For Case F15, the temperature of the jet head increases, and the fuel-air mixing increases toward stoichiometry, enhancing chemical reactions to support flame expansion. The diffusion flame (DF) and premixed flame (PF) propagate in opposite directions. However, the initially formed PF extinguishes at $t = 27$ ms mainly due to the low temperature of the jet center with rich cryogenic hydrogen concentration, as shown by the disappearance of flame front scaled by the bule circle in Fig. 13(b). The DF propagates to surround the jet head. The high-temperature region expands in the jet flow because of the

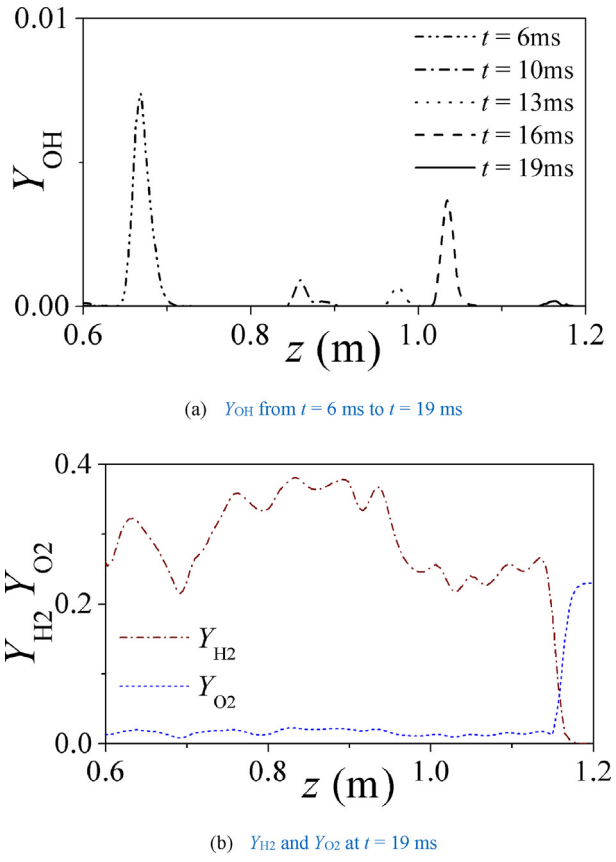

Fig. 9 – Streamwise profiles along the centerlines for Case F05: (a) Y_{OH} from t = 6 ms to t = 19 ms, and (b) Y_{H2} and Y_{O2} at t = 19 ms.

heat transfer from combustion products of DF. In the core region, some spontaneous FKs are generated with a premixed mode, as shown by the scatted distributions of FKs in Fig. 13(c), but they disappear subsequently. Unburnt cold mixture still accumulates in the core region. The FK formed inside the jet cannot sustain, but the FK generated around the edge of the jet spontaneously can expand to form a stable premixed flame, shown by the snapshots at the time of 32 ms and 34 ms. The premixed mixture inside the jet has a higher fuel concentration and a much lower temperature, which inhibit flame propagation. The flame shows a dominant diffusion feature while its lower section has some premixed feature as shown in Fig. 13(f) and Fig. 14(f).

As the ignition position moves further downstream to z_{ig} = 2.0 m, the jet flame lift-off distance further increases, as shown in Fig. 10(c). After a flame kernel is grown, a diffusion flame and a premixed flame are formed, respectively as shown in Fig. 15(a). The DF propagates with the dispersion of the jet tip. The PF propagates towards the cold fuel-rich mixture inside the jet. Subsequently, the PF extinguishes due to localized high fuel concentration and very low temperature, as highlighted in Fig. 15(b). The DF expands outside to envelop the jet head. The propagation trajectory is close to the stoichiometric condition. The shear around the jet promotes mixing and generates reactive pockets on the outer edge of the jet. The DF expands faster than the inner flame as the local velocity is relatively small. Due to the inhomogeneous spatial distribution of the hydrogen concentration, the flame surface tends to become corrugated. The expansion of DF starts to speed up from time 58 ms–60 ms as the wrinkling of the flame front increases the flame surface area. This, in turn, increases the hydrogen consumption rate and provides additional acceleration of the flame. Premixed flames are formed as the vortex entrains the reactive mixtures upstream at 58 ms as marked by PF in Fig. 15(c). Then the PF propagates toward the central region of the jet and the shape of the overall flame area tends to be a semicircle, which is also found in the experiment, as shown in Fig. 16. The distributed flame kernels are formed around the bottom of the flame. Comparing to the near-field ignition, the spontaneously formed FKs for Case F20 expand to connect with the main flame to extend the flame area, as shown by the snapshots from times 62 ms–64 ms. For the far-field ignition (Case F15

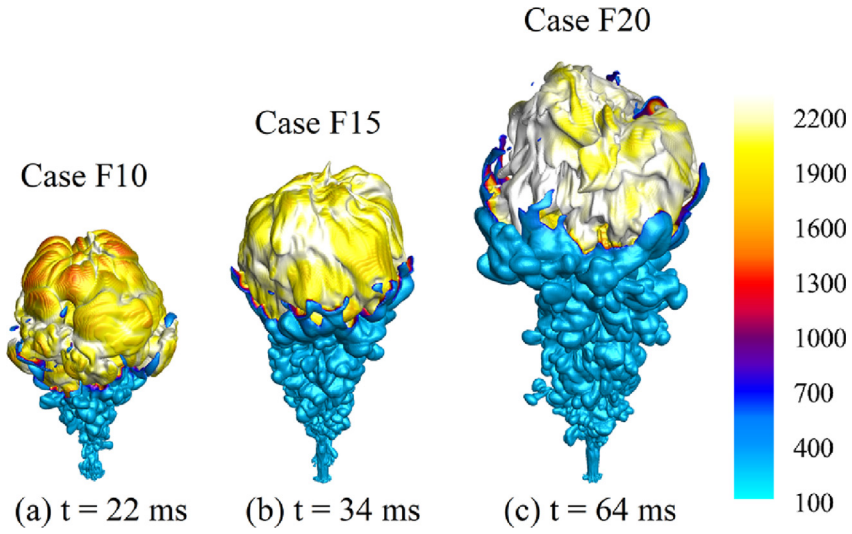

Fig. 10 – Flame structure of ignited jet for Case F10, Case F15, and Case F20 marked using X_{H2} = 0.04 iso-surface colored by temperature (K).

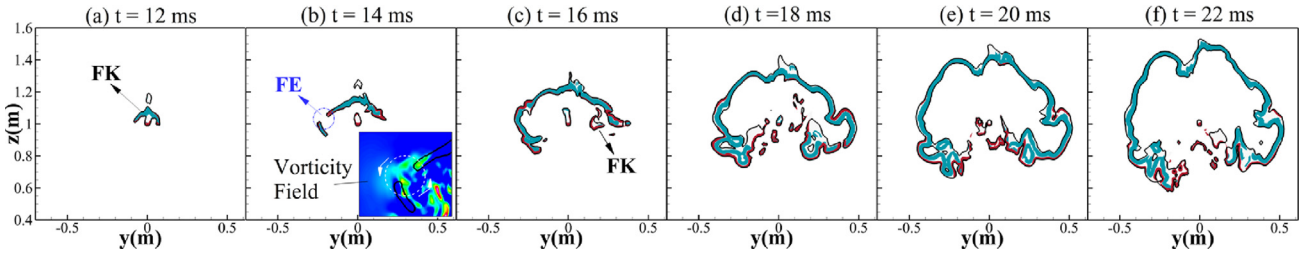

Fig. 11 – Evolution of flame structure at the y-z middle-plane for Case F10. The annotations are the same as Fig. 6.

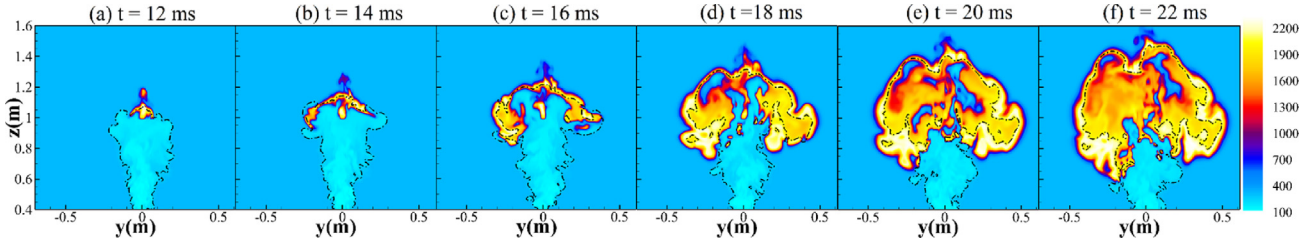

Fig. 12 – Evolution of combustion field at the y-z middle-plane for Case F10. The annotations are the same as Fig. 7.

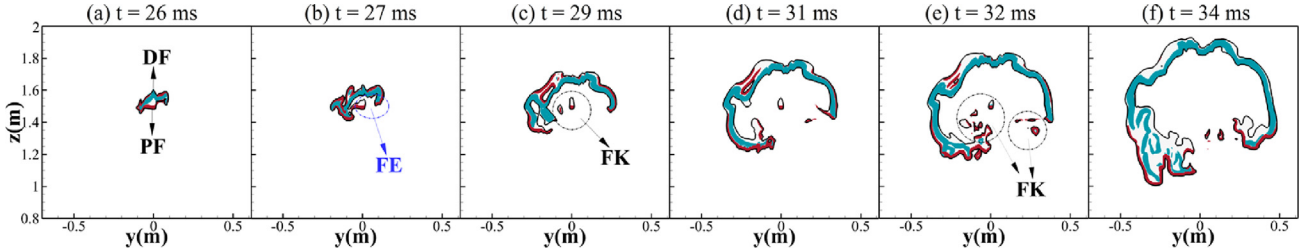

Fig. 13 – Evolution of flame structure at the y-z middle-plane for Case F15. The annotations are the same as Fig. 6.

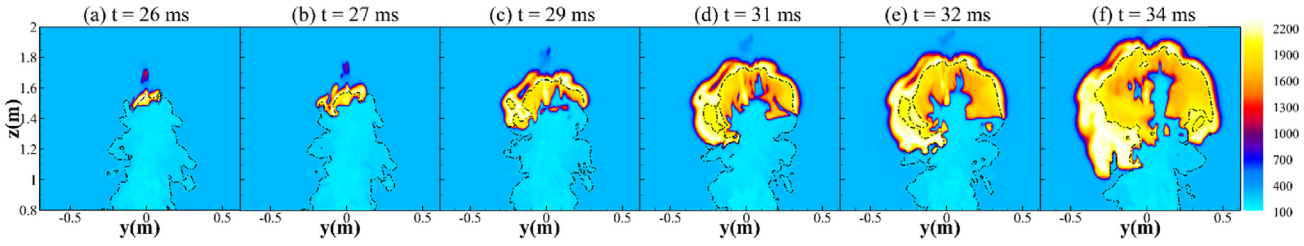

Fig. 14 – Evolution of combustion field at the y-z middle-plane for Case F15. The annotations are the same as Fig. 7.

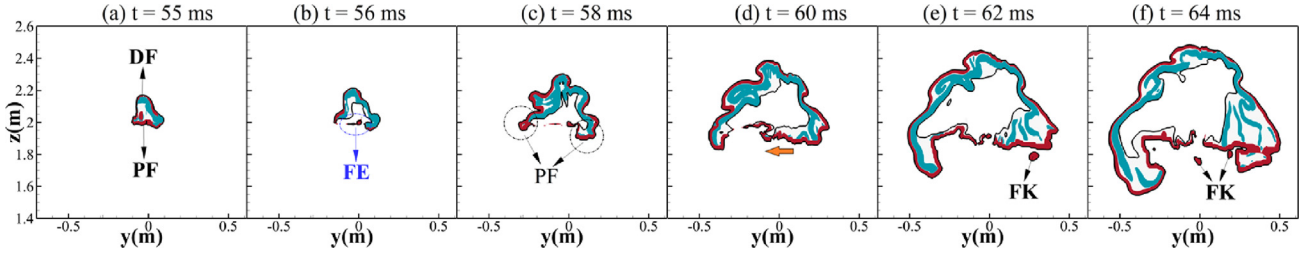

Fig. 15 – Evolution of flame structure at the y-z middle-plane for Case F20. The annotations are the same as Fig. 6.

and Case F20), the hydrogen and surrounding oxygen form a premixed reactive mixture before interacting with the ignition source. The overall flame contains a diffusion flame on the outer edge of the jet and a premixed flame inside the jet. An envelope flame structure is formed for the cryogenic hydrogen jet ignited at 1.5 and 2.0 m.

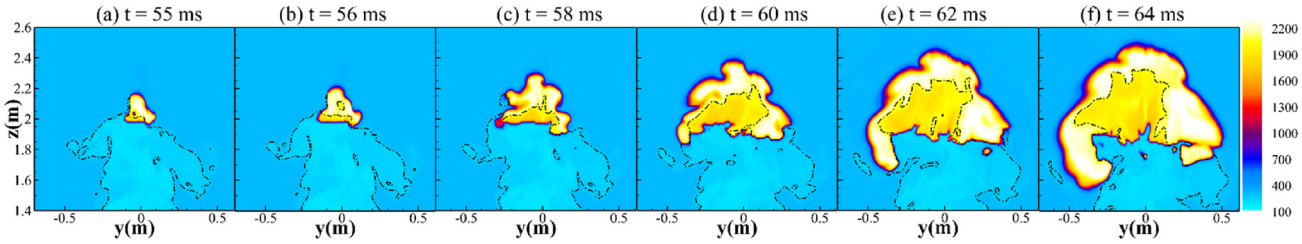

Fig. 16 – Evolution of combustion field at the y-z middle-plane for Case F20. The annotations are the same as Fig. 7.

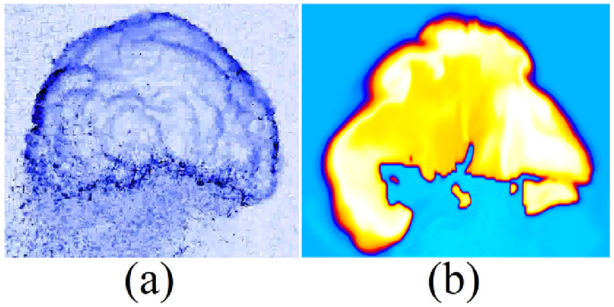

Fig. 17 – Snapshots of the flame shapes: (a) experiment (reproduced from [20]) and (b) Case F20.

It should be noted that there was an ignition delay of 40–160 ms in the experiments [14]. The present simulations were set up before the experiments were performed. Ignition was started right at the beginning. Because of this difference, it is not possible to compare the predicted and measured maximum overpressures directly. However, some qualitative comparison is still possible. The semicircle-shape flame was recorded in the test for ignition at z_{ig} = 2.0 m, as shown in Fig. 17(a). This is similar to the predicted evolution of the temperature contours in Fig. 17(b). Deflagration waves were captured in the predictions for the far-field ignited jets (F15 and F20), which were also observed in the experiment, as shown in Fig. 18(a).

In summary, the present predictions show that the ignition location, z_{ig}, has considerable influence on the flame structure. For the considered near-field ignition location (z_{ig} = 0.5 and 1.0 m), the flame kernel grows from the ignition source and propagates around the outer edge of the jet, forming a diffusion flame on the sides of the jet. The shear between the high-speed jet and ambient air promotes hydrogen-air mixing and generates reactive pockets for combustion. The local backflow from the rotating vortex formed in the shear turbulence also supports the propagation of the diffusion flame. Therefore, the expansion of the diffusion flame can be regarded as a turbulence controlled. Due to the relatively low temperature inside the jet, the cold mixture cannot be ignited. The area of the unreacted mixture decreases with the increase of z_{ig}. For the far-field ignition (z_{ig} = 1.5 and 2.0 m), a diffusion flame engulfs the periphery of the jet like that in the near-field ignition. The fuel concentration decreases toward the stoichiometry and the temperature of the mixture in the main jet increases with the increase of the distance from the nozzle. These conditions are favorable to the formation of flame kernels. Spotted premixed flame kernels grow spontaneously inside the jet and expand to form a premixed flame. Initially, the premixed flame propagates at lower speed than the diffusion flame because of the lower local relative velocity. Deflagration waves were captured in the predictions for these two cases.

Conclusions

Transient evolution of flame in ignited high-pressure cryogenic hydrogen jets is investigated numerically using LES with detailed chemistry. Full sequence of the ignition kernel development is computationally captured for four cases with different ignition locations. The resulting flames show different propagation characteristics. For ignition at 0.5 and 1.0 m from the nozzle, the flame cannot propagate inside the cold jet and a side diffusion flame is formed. For ignition at 1.5 and 2.0 m from the nozzle, an envelope flame with mixed diffusion and premixed combustion modes is formed around the jet, which is attributed to the improved hydrogen-air mixing and higher temperature in the downstream region.

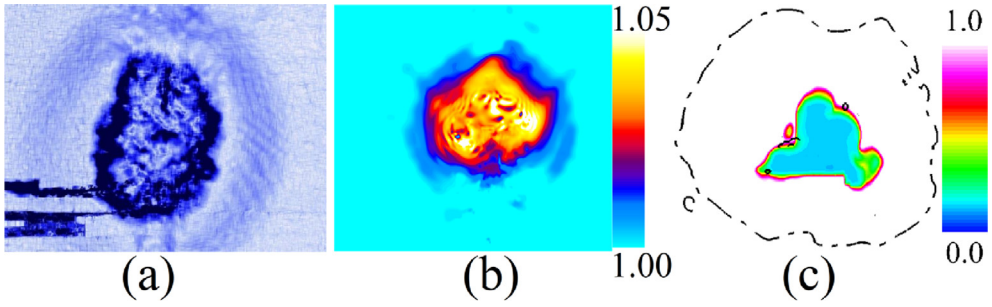

Fig. 18 – Snapshot of the deflagration waves: (a) experimentally observed (reproduced from [20]), (b) predicted pressure contour for Case F15, (c) predicted density contour (kg/m^3) with static pressure iso-line of 1.03 atm.

Localized spontaneous ignition and transient flame extinguishment during flame evolution have been captured, and attributed to the complex interactions between turbulence, fuel-air mixing at cryogenic temperature and chemical reactions. Deflagration waves have been captured in the far-field ignited jets, implying potential for explosion in the cases of delayed ignition.

Declaration of competing interest

The authors declare that they have no known competing financial interests or personal relationships that could have appeared to influence the work reported in this paper.

Acknowledgments

The authors acknowledge financial support from the Fuel Cells and Hydrogen Joint Undertaking under the EU's Horizon 2020 research and innovation program for the PRESLHY project (Grant No.779613). The simulations used the HPC facility ARCHER2 through UK Consortium on Turbulent Reacting Flows (UKCTRFEP/R029369/1).

REFERENCES

[1] Cirrone DMC, Makarov D, Molkov V. Thermal radiation from cryogenic hydrogen jet fires. Int J Hydrogen Energy 2019;44:8874–85.
[2] Giannissi SG, Venetsanos AG. Study of key parameters in modeling liquid hydrogen release and dispersion in open environment. Int J Hydrogen Energy 2018;43(1):455–67.
[4] Veser A, Kuznetsov M, Fast G, Friedrich A, Kotchourko N, Stern G, Schwall M, Breitung W. The structure and flame propagation regimes in turbulent hydrogen jets. Int J Hydrogen Energy 2011;36:2351.
[5] Friedrich A, Breitung W, Stern G, Veser A, Kuznetsov M, Fast G, Oechsler B, Kotchourko N, Jordan T, Travis J. Ignition and heat radiation of cryogenic hydrogen jets. Int J Hydrogen Energy 2012;37:17589.
[6] Panda PP, Hecht ES. Ignition and flame characteristics of cryogenic hydrogen releases. Int J Hydrogen Energy 2017;42:775–85.
[7] Hecht ES, Chowdhury BR. Characteristic of cryogenic hydrogen flames from high-aspect ratio nozzles. Int J Hydrogen Energy 2021;46:12320–8.
[8] Chowdhury BR, Hecht ES. Dispersion of cryogenic hydrogen through high-aspect ratio nozzles. Int J Hydrogen Energy 2021;46:12311–9.
[9] Venetsanos A, Giannissi S. Release and dispersion modeling of cryogenic under-expanded hydrogen jets. Int J Hydrogen Energy 2017;42:7672–82.
[10] Ren Z, Wen JX. Numerical characterization of under-expanded cryogenic hydrogen gas jets. AIP Adv 2020;10. 095303.
[11] Giannissi SG, Venetsanos AG, Hecht ES. Numerical predictions of cryogenic hydrogen vertical jets. Int J Hydrogen Energy 2021;46:12566–76.
[12] Ba Q, He Q, Zhou B, Chen M, Li X, Cheng L. Modeling of cryogenic hydrogen releases. Int J Hydrogen Energy 2020;45:31315–26.
[13] Cirrone D, Makarov D, Kuznetsov M, Friedrich A, Molkov V. Effect of heat transfer through the release pipe on simulations of cryogenic hydrogen jet fires and hazard distances. Int J Hydrogen Energy 2022;47(12):21596–611.
[14] Jordan T, Bernard L, Cirrone D, Coldrick D, Friderich A, Jallais A, et al. Results of the pre-normative research project PRESLHY for the safety use of liquid hydrogen. Procedings of 9th Int. Conf. on Hydrogen Safety. Sep. 2021:189–207 [Edinburgh, UK]. In this issue.
[15] Keenan J, Makarov D, Molkov V. Modelling and simulation of high-pressure hydrogen jets using notional nozzle theory and open source code OpenFOAM. Int J Hydrogen Energy 2017;42:7447–56.
[16] Yoshizawa A. Bridging between eddy-viscosity-type and second-order turbulence models through a two-scale turbulence theory. Phys Rev E 1993;48:273.
[17] Parente A, Malik MR, Contino F, Cuoci A, Dally BB. Extension of the Eddy Dissipation Concept for turbulence/chemistry interactions to MILD combustion. Fuel 2016;163:98–111.
[18] Ó Conaire M, Curran HJ, Simmie JM, Pitz WJ, Westbrook CK. A comprehensive modeling study of hydrogen oxidation. Int J Hydrogen Energy 2004;36:603–22.
[19] Shelke AV, Wen JX. The burning characteristics and flame evolution of hydrocarbon and hydrogen flash fires. Proc Combust Inst 2021;38:4699–708.
[20] Friedrich A, Veser A, Necker G, Gerstner J, Kotchourko N, Kuznetsov M, Jordan T. Characterization of high-pressure cryogenic hydrogen jet fires (ignited DISCHA). PRESLHY Dissemination Conference 2021;5-6. May.
[21] Friedrich A, Veser A, Kotchourko N, Kuznetsov M, Jordan T. High-pressure cryogenic hydrogen releases (unignited DISCHA). PRESLHY Dissemination Conference 2021;5-6. May.
[22] McGrattan K, Hostikka S, McDermott R, et al. Fire dynamics simulator user's guide. NIST Spec Publ 2013;1019(6):1–339.
[23] Chen Z, Ruan S, Swaminathan N. Large eddy simulation of flame edge evolution in a spark-ignited methane–air jet. Proc Combust Inst 2017;36:1645.
[24] Mizobuchi Y, Shinjo J, Ogawa S, Takeno T. A numerical study on the formation of diffusion flame islands in a turbulent hydrogen jet lifted flame. Proc Combust Inst 2005;30:611–9.
[25] Burali N, Lapointe S, Bobbitt B, Blanquart G, Xuan Y. Assessment of the constant non-unity Lewis number assumption in chemically-reacting flows. Combust Theor Model 2016;20(4).
[26] Wang CJ, Wen JX, Chen ZB, Dembele S. Predicting radiative characteristics of hydrogen and hydrogen/methane jet fires using FireFOAM. Int J Hydrogen Energy 2014;39(35):20560–9.
[27] Wierzba I I, Ale BB. Effects of temperature and time of exposure on the flammability limits of hydrogen-air mixtures. Hydrogen Power: theoretical and Engineering Solutions. Dordrecht: Springer; 1998. p. 69–74.
[28] Proust C, Jamois D. Some fundamental combustion properties of "cryogenic" premixed hydrogen air flames. In: Int. Conference on hydrogen safety. Edinburgh, UK; Sep. 2021.